Frequency Modulated Interrupted Continuous Wave as Wall Removal Technique in Through-The-Wall Imaging

Francesco Fioranelli, Sana Salous, and X. Raimundo
Centre for Communications Systems, School of Engineering and Computing Sciences, Durham University, Durham, DH1 3LE, United Kingdom
E-mail: {francesco.fioranelli, sana.salous, x.z.raimundo}@durham.ac.uk

Abstract— Undesired wall reflections in through-the-wall imaging can mask the return from actual targets and saturate and block the receiver. We propose frequency modulated interrupted continuous wave (FMICW) signals as a novel wall removal technique and validate its effectiveness through numerical simulations and experiments performed using a radar system built for the purpose. FMICW waveforms appear to mitigate wall reflections and benefit the through-wall detection of stationary targets and of people moving or breathing behind different kinds of wall.

Keywords— UWB radar, through-the-wall imaging, FMCW, FMICW

I- INTRODUCTION

THROUGH-THE-WALL-DETECTION (TTWD) techniques have been investigated in the past few years as a way to support police and soldiers operating in urban areas (e.g. when breaking in a room occupied by hostile agents) and to help first responders in search and rescue operations (e.g. when looking for people trapped inside buildings on fire or buried under rubble). Ultra wide band (UWB) microwave signals proved to be a mature technology for TTWD, since they can provide suitable through-wall penetration and range resolution for imaging purposes, provided that the frequency range of the waveform is appropriate [1]. Wide bandwidth is indeed required to achieve fine down-range resolution and low operational frequency is desired to reduce through-wall propagation losses, even if this implies bulkier antennas which may be inappropriate for in-field applications. An effective compromise in the choice of the bandwidth must be sought when designing radar systems for TTWD, as well as taking into account constraints like weight, size, and power consumption of the system.

Many radar systems have been presented in the literature and successfully validated for a variety of applications such as through-wall detection of stationary targets, tracking people while walking behind walls, and detection of people through their breathing. Different UWB waveforms have been used in these systems, including short impulses [2-4], noise [5] and pseudo-noise waveforms based on M-sequences [6], stepped frequency continuous wave (SFCW) signals [7-9], and frequency modulated continuous wave (FMCW) signals [10-15].

Wall reflections compromise the through-wall detection of possible targets in active radar systems. Depending on the dielectric permittivity contrast, the presence of the air/wall interface scatters back most of the transmitted signal and drastically reduces the amount of power available to sense the area under test. Therefore at the receiver wall reflections appear far stronger than the backscattered signals from actual targets, especially from targets with low radar cross section (RCS) such as human beings, which are masked and difficult to detect. Walls with air gaps or hollow structures are especially challenging, since they tend to trap the electromagnetic waves as if in resonant cavities, making the duration of the wall reflection signals far longer than the physical thickness, thus overshadowing targets close to the interior wall [11, 16]. The presence of strong undesired signals limits the dynamic range of the TTWD system and increase the possibility of saturating and blocking the receiver [12]. Furthermore it has been observed that this prevents the application of compressive sensing (CS) techniques, which aim at producing radar images of same quality and resolution using far fewer data, thus allowing faster measurements [17].

Several wall removal techniques have been presented in the literature to deal with the aforementioned problem. Subspace projection techniques aim at separating the clutter sub-space (including antenna cross-talk and wall reflections) from the target sub-space through suitable decomposition methods applied to the data; the clutter sub-space is then discarded when generating radar images [18-19]. Spatial filtering approach considers an array of receivers parallel to the wall and assumes that wall reflections are similar at every receiver along the array, whereas the contribution of echoes from the targets changes. Signals related to the wall can be separated from those related to the actual targets by applying a spatial frequency transform to convert the data into the new spatial frequency domain; a filter is then applied to the data to remove wall

reflections [16]. An alternative method isolates wall reflections from the received signal and extracts the required parameters to compute analytically the response of the wall, which is then subtracted from the actual measured data [20].

Change detection (CD) techniques can be applied if the radar system aims at motion detection. The assumption is that stationary clutter, including wall reflections, does not change while performing measurements with moving targets; undesired signals can therefore be removed by simply subtracting data referring to different measurement instants. This subtraction can be performed either on raw data (coherent subtraction) [4-5], or on images after the application of beam-forming algorithms (non-coherent subtraction) [9]. The stationary background to be subtracted from the data can be estimated with more refined methods, for instance averaging the previous received signals [2], or with suitable weights to cope with targets that stop for a while during the measurement [3].

Another wall removal technique for radar systems using FMCW waveforms is based on band-pass filtering the beat-note signal before digitization; this signal contains information on the distance of the targets in frequency components proportional to the distance itself. Since the wall is physically closer to the radar system in comparison with the targets, its contribution appears at lower frequency components, which can therefore be filtered out with a suitable band-pass filter integrated at the receiver [10-15]. In [15] for instance, coherent change detection and band-pass filtering are combined on a vehicle-mounted system. This system is able to detect the presence of human targets standing still and holding breath behind a variety of different walls, like 10 cm thick solid concrete and cinder blocks.

Results from numerical simulations show that reflections from walls and from people could be distinguished by their polarization, the former being mostly co-polarized with the transmitted signal, the latter mostly cross-polarized because of the irregular shape of human bodies [21]. However the practical exploitation of cross-polarized components is limited because they are far weaker than co-polarized components and the generation and reception of pure polarizations through typical antennas for through-wall detection is challenging [22].

In this paper we present an alternative wall removal technique for through-wall detection based on frequency modulated interrupted continuous wave (FMICW) waveforms; although used in the past for ocean sensing radar systems and ionospheric channel sounding, these signals have not been used yet in TTWD scenarios to the best of our knowledge. FMICW waveforms are switched on and off at the transmitter providing listening intervals at the receiver, which is switched with a complementary pattern; using suitable switching patterns it is possible to ensure that these listening intervals do not include undesired wall reflections, which are therefore attenuated or removed at the receiver.

A detailed description of the proposed wall removal technique is provided in this paper, with an extensive validation through results from numerical simulations and different experiments. This paper is organized as follows. In section II FMICW signals are analytically described and potential advantages and disadvantages discussed in relation with other existing wall removal techniques. In section III results from numerical simulations performed to validate FMICW signals in TTWD scenarios are presented, comparing radar profiles and images obtained using normal FMCW waveforms and proposed FMICW waveforms. In section IV the experimental validation of the proposed technique in realistic scenarios is provided with results from a back-to-back test and from tests aiming at through-wall detection of stationary targets and detection of people through their movement and breathing. More information when comparing FMICW approach and other hardware wall removal methods is also provided, together with the description of the radar system developed for the measurements. Finally section V concludes this paper.

II- FMICW WAVEFORMS

FMICW signals date back to the eighties for applications such as ionospheric channel sounding and ocean surface sensing, for which monostatic approach with one single antenna operating at the same time at the transmitter and at the receiver would be preferable [23]. A recent survey of existing oceanographic radar networks across the Pacific coastal area shows that several systems are still based on FMICW signals [24].

FMICW signals are generated by switching on and off with complementary sequences the transmitter and the receiver of a normal FMCW radar system to ensure that they are not simultaneously active. These gating

sequences can be mathematically modelled through binary functions with bit duration T_B which multiply the transmitted and received FMCW signals; the transmitter/receiver is off when the value of the binary functions is 0 and on when the value is 1. The effect of the use of these gating sequences can be investigated through the mean received signal (MRS), which is the cross-correlation between the sequence g(t) applied at the transmitter and the complementary 1-g(t) applied at the receiver, as in (1) where T_S denotes the overall duration of the sequence:

$$MRS(\tau) = \frac{1}{T_S}\int_0^{T_S} g(t-\tau)\,[1-g(t)]dt \tag{1}$$

The MRS is therefore a property of the gating sequence, depending on its bit duration and number of bits, being T_S equal to T_B multiplied by the number of bits N. The MRS depends also on the round-trip delay τ, i.e. the time for the transmitted signal to reach the targets in the area under test and be backscattered to the receiver; this time is related to the spatial distance of the targets. Therefore the MRS can be considered a sort of distance dependent weight applied to the received power. For some values of distances the MRS pattern provides additional attenuation (when the receiver is not listening), for other values there is no additional attenuation (when the receiver is listening). By carefully designing the sequences, it is possible to get MRS patterns suitable for wall removal in TTWD applications, i.e. patterns which provide attenuation at distances corresponding to wall reflections and do not alter the received power at distances corresponding to the area under test.

The MRS is zero when the round-trip delay τ is multiple of the sequence duration T_S, generating blind ranges where the received power is zero. The duration of the gating sequence should therefore be longer than the round-trip delay related to the farther target expected in the scenario under test τ_{MAX}; this ensures that there are no blind ranges within the area of interest. This condition can be written as in (2):

$$T_S = NT_B > \tau_{MAX} \tag{2}$$

The multiplication of FMCW signals and gating sequences to generate FMICW waveforms corresponds to spectral convolution in the frequency domain. Being periodic signals, the spectrum of the gating sequences is a train of impulse functions placed at every multiple of the reciprocal of the sequence duration T_S, which we can call f_S. The spectrum of the original FMCW signal is replicated at the positions of these impulse functions as an effect of the convolution. The sequence frequency f_S should therefore be higher than twice the highest expected frequency component of the beat-note signal at the receiver f_{BMAX} in order to avoid aliasing and distortion of the spectrum. This condition can be written as in (3), where the maximum beat-note frequency is expressed in terms of bandwidth B and duration T of the FMCW signal, and of the maximum distance of the target R_{MAX} (assuming monostatic approach for simplicity):

$$f_S > 2f_{BMAX} \equiv T_B < \frac{cT}{4BNR_{MAX}} \tag{3}$$

Equations (2) and (3) set a constraint on the choice of the gating sequence parameters, namely number of bits N and their duration T_B, given bandwidth and duration of the FMCW signal and the maximum expected target distance.

When using FMICW waveforms, the off-time at the transmitter and at the receiver reduces the system signal-to-noise ratio (SNR) in comparison with normal FMCW waveforms. It has been shown that gating sequences with 50% duty cycle provide maximum power efficiency, thus minimizing the reduction of SNR [25]. However gating sequences with lower duty cycle at the receiver may be useful in TTWD applications to extend the blind ranges in the MRS patterns, thus having more effective wall removal.

Fig. 1 and 2 show the gating sequences used on the simulated and experimental data presented later in this paper, a square wave and a 3 bit M-sequence, respectively. Fig. 3 shows the corresponding MRS patterns. Two additional delays τ_{RX1} and τ_{RX2} are used to change the duty cycle of the sequence applied at the receiver, thus extending the blind ranges in the MRS. In Fig. 3 two blind ranges can be seen for both MRS, the first at the beginning of the pattern and depending on the parameter τ_{RX2}, and the second at the end of the first period of the sequence (bit 2 for the square wave and bit 3 for the M-sequence), depending on both τ_{RX1} and τ_{RX2}. As

mentioned, longer τ_{RX1} and τ_{RX2} would produce longer blind ranges for more effective removal of wall reflections but would also reduce the system SNR. Therefore a compromise must be sought.

We believe that FMICW waveforms can be an interesting wall removal technique, presenting some potential advantages compared with other existing methods. Unlike subspace projection and spatial filtering, FMICW waveforms remove wall reflections before the digitization of the beat-note signal, thus avoiding the reduction of the system dynamic range and the possibility of blocking the receiver. FMICW waveforms are not subject to estimation or modelling errors in comparison with the approach of extracting the wall response from the data and then subtracting it. Change detection approaches are not suitable for detection of stationary targets and are applied after digitization of the signal, thus not addressing the reduction of dynamic range at the receiver.

Therefore only hardware approaches like FMICW through the MRS of the gating sequences, or band-pass filtering can solve the dynamic range issue, as a round-trip delay dependent attenuation is provided to remove the undesired components. However, these approaches do not address the problem of ringing generated by some types of walls with cavities and internal hollow structures. In these cases, part of the late wall reflection or its multiple copies, are overlapped with the wanted return from targets close to the wall. The application of hardware methods would attenuate both wall and targets return without addressing the problem of discriminating between them. Hardware methods like FMICW waveforms can also be combined with other aforementioned wall removal techniques, such as subspace projection, spatial filtering, and change detection, in order to remove residual wall reflections, thus improving the overall performance of the system.

III- NUMERICAL SIMULATIONS OF FMICW WAVEFORMS

Numerical simulations of realistic TTWD scenarios have been performed using CST Microwave Studio to validate the proposed FMICW waveforms as wall removal technique; the method finite integration in time domain (FIT) has been chosen as it is the best choice for electrically large, non-resonant, and detailed structures. Simulated scenarios include tridimensional rooms with potential targets inside, namely a metallic cabinet and a human phantom. The rooms have realistic size of about 4-5 m^2; ceiling and floor have been also

simulated for increased realism and to avoid artifacts caused by the waveform diffraction at the top and bottom edges of the wall [26]. The human phantom is modeled with a uniform material reproducing the electrical parameters of human skin, as it has been observed that at the frequency range relevant for TTWD applications most of the electromagnetic power is reflected by the skin without penetration into the body. Therefore there is no need to model internal tissues, thus reducing the computational burden of the simulations in terms of memory and CPU time [27]. The transmitter is modeled for simplicity as a plane wave, whereas the receivers are modeled as probes which sample and record electromagnetic fields; the images shown in this paper are created using 9 probes, which are placed 25 cm apart, thus forming a 2 m long array. The signal has 1.5 GHz bandwidth in the range 0.5-2 GHz, corresponding to range resolution 10 cm.

Three imaging algorithms are used to create the radar images shown in this paper. They are the well-known back projection (BP) algorithm [28], and the delay-sum-integration (DSI) or the delay-multiply-sum-integration (DMSI), which were originally proposed for medical imaging [29-30]. An incorrect estimation of the round-trip delay for the transmitter-pixel-receiver path when applying these algorithms would lead to blurring and displacement in the radar images. The actual values of round-trip delay depend on the length of the propagation path within the wall, where the propagation speed of the signal is reduced proportionally to the permittivity of the wall material. Accurate estimations of the through-wall propagation path have been presented in the literature [31], but in this paper we adopt a simplified approach which avoids solving transcendental equations. This approach does not take into account the refraction at the interface between wall and air, thus considering straight-ray trajectories for the through-wall propagation of the waveforms. The round-trip delay can be written as the sum of the part related to the transmitter-pixel path τ_{TX} and the pixel-receiver path τ_{RX}.

Since the transmitter is modelled by a plane wave in our numerical simulations, the excitation wavefront is uniform for every pixel in the area under test and the wave impinges perpendicularly to the wall. The estimation of τ_{TX} is therefore easy as the actual through-wall propagation path is the thickness of the wall D, as in (4):

$$\tau_{TX} = \frac{R_{TX}}{c} + \frac{D}{c}\sqrt{\varepsilon_r - 1} \tag{4}$$

R_{TX} is the transmitter-pixel distance, which in case of plane wave excitation is the distance from the pixel to the boundary of the simulated volume where the plane wave ideally starts to propagate. It should be noted that the first term in (4) refers to the free space case, with the second term correcting for the presence of the wall. Equation (5) shows the estimation of τ_{RX} where the first term refers to the free space delay for the pixel-receiver path, and the second term corrects for the presence of the wall assuming straight-ray approximation, with L through-wall propagation path and θ the angle between the pixel-receiver path and the perpendicular to the wall. This angle can be computed from the coordinates of pixel and receiver as in (6), with reference to the simplified geometry shown in Fig. 4.

$$\tau_{RX} = \frac{R_{RX}}{c} + \frac{L}{c}\sqrt{\varepsilon_r - 1} = \frac{R_{RX}}{c} + \frac{D}{c \cdot cos\theta}\sqrt{\varepsilon_r - 1} \tag{5}$$

$$\theta = arctg\left(\frac{|y_p - y_r|}{|x_p - x_r|}\right) \tag{6}$$

Results from two different simulated scenarios are presented in this paper. A view of the first scenario is shown in Fig. 5, where the points with arrows on the left are the probes which model the receivers. The size of the room is 235 cm × 200 cm and the stand-off distance of the probes from the exterior wall is 250 cm, corresponding to 16.67 ns round-trip delay in free space. The material used for walls, ceiling, and floor is 1 year old solid concrete, with permittivity 5.657 at the centre frequency 1.25 GHz. The wall is solid and 15 cm thick. The duration of the simulated waveform is 3000 ns, so that the maximum allowed bit duration from the anti-aliasing condition in (3) is 25/N ns, assuming a gating sequence with N bits and maximum distance 6 m. The distance from the probes is 440 cm for the cabinet and 370 cm for the human phantom, corresponding to free space round-trip delay 29.33 ns and 24.67 ns, respectively. The values of these round-trip delays are actually higher if the slower propagation speed within the wall is taken into account. Given the permittivity and the thickness of the wall in this simulated scenario, the actual values of delays are 30.7 ns and 26.04 ns, for the cabinet and the phantom, respectively.

In Fig. 6 two radar profiles from the first simulated scenario are presented, using FMCW and FMICW waveforms respectively. Both profiles refer to the signals recorded at a probe facing the metallic cabinet target and are normalized to the maximum of the FMCW profile, which is the reflection from the outer air-wall interface. The gating sequence used for FMICW waveforms is the 3 bit M-sequence shown in Fig. 2 and with MRS shown in Fig. 3. The bit duration is 5.75 ns and the delays τ_{RX1} and τ_{RX2} are equal to 1.5 ns. The second blind range of the MRS is used for wall removal as it is centred at 17.25 ns and 3 ns long, with the round-trip delay corresponding to the wall equal to 16.67 ns. The reflection from the human phantom (at 26.04 ns) is in the flat area of the MRS where no additional attenuation is given, whereas the reflection from the cabinet (at 30.7 ns) is on the slope of the MRS, but the additional attenuation does not compromise the detection of this target, which has higher RCS compared with the human phantom. In the FMCW profile the return from the cabinet target is about 14 dB below the reflection from the outer wall interface and 7 dB below the reflection from the inner wall. In the FMICW profile the outer wall interface is completely blanked by the gating sequence, and the target reflection is the strongest return in this profile, being roughly 6 dB above the residual of the inner wall interface. In absolute terms, the magnitude of the FMICW profile is lower compared with the FMCW profile because of the attenuation of the received power due to switching sequence, as previously mentioned in section II. For the gating sequence used in this scenario, the receiver on-time is only 2.75 ns over 17.25 ns, which corresponds to 16 dB additional attenuation on the flat part of the MRS. This is the value of magnitude attenuation for the cabinet target return in the FMICW profile compared with the FMCW profile, as it can be seen in Fig. 6, bearing in mind that the actual attenuation is slightly higher because the target reflection is on the slope of the MRS. When performing actual experiments, this additional attenuation can be compensated at the receiver. Fig. 7 compares radar images obtained from the first simulated scenario using normal FMCW waveforms and the proposed FMICW waveforms; both BP and DMSI imaging algorithms have been used. Fig. 7a confirms that using FMCW waveforms wall reflections are the strongest contribution in the radar image, even if it is possible to locate the targets with a sufficiently large dynamic range of the colour scale. With the application of the gating sequences as in Fig. 7b, the wall reflection contribution can be strongly attenuated so that its magnitude is lower or comparable with the target reflections magnitude. Therefore the targets appear brighter in comparison with the wall residual in the FMICW image

compared with the FMCW image. Comparing the FMICW results from the two imaging algorithms, we can see that DMSI attenuates the artefacts in yellow close to the human phantom and produces coloured spots which are better focused on the actual position of the targets.

In the second simulated scenario the stand-off distance is reduced to 25 cm and the material for walls, ceiling, and floor is 40 years old concrete, with permittivity 4.642 at the centre frequency 1.25 GHz. The size of the room is 290 cm × 170 cm and the wall is solid and 15 cm thick as in the previous scenario. The targets are two human phantoms, one facing the array of probes with the chest and one with the back, placed at roughly 160 and 240 cm from the probes. The duration of the simulated waveform is increased to 5000 ns, thus having maximum allowed bit duration 50/N ns from (3), assuming N bits for the gating sequence and maximum expected distance of the target 5 m. Fig. 8 shows a view of this scenario.

The free space round-trip delay corresponding to the stand-off distance and to the distance of the two targets is 1.67 ns, 10.67 ns, and 16 ns respectively. Two different gating sequences have been tested in this scenario, namely the square wave with bit duration 16 ns and the 3 bit M-sequence with bit duration 8.75 ns; the MRS of these sequences can be seen in Fig. 3 where the delays τ_{RX1} and τ_{RX2} are assumed to be zero . The MRS of the M-sequence provides no attenuation at the values of round-trip delay related to the two targets, whereas wall reflections are mitigated by the first blind range at the beginning of the MRS. The MRS of the square wave has a maximum with no attenuation at the round-trip delay corresponding to the far target, 16 ns, whereas both wall reflections and the echo from the close target are attenuated by the slope of the MRS. The overall effect is an enhancement of the reflections from the far target to compensate for its greater distance.

Fig. 9 shows radar images obtained from the second simulated scenario using different waveforms and different algorithms. Fig. 9a and 9b compare results using normal FMCW and FMICW waveforms gated with the M-sequence; in both cases the images are formed using BP algorithm. As in the previous scenario, in the FMCW case the contribution from the wall is the strongest return in the image, whereas in the FMICW case the targets contributions have larger or comparable magnitude with respect to the residual wall reflections, and therefore they appear brighter in the image. In Fig. 9b and 9c the same FMICW waveforms is used but with different imaging algorithms, BP and DMSI respectively. We can see that DMSI produces coloured spots

much better focused on the actual position of the targets and attenuates the residual wall reflection, as it is weaker than the echoes from the targets. In Fig. 9c the echo from the far target appears rather weak in comparison with the close target. In Fig. 9d the application of the square wave as gating sequence for FMICW waveforms enhances the detection of the far target due to the maximum MRS at its corresponding round-trip delay.

These results from simulated data validate the effectiveness of the proposed FMICW waveforms as wall removal technique. The second blind range in the MRS of suitable gating sequences can be exploited to mitigate wall reflections in case of long stand-off distances as in the first scenario, or the first blind range for shorter distances as in the second scenario. It has been also shown how square waves with suitable bit duration can be applied to enhance the detection of far targets with low RCS.

IV- Experimental Validation of FMICW Waveforms

A radar system has been built to validate the proposed FMICW waveforms through experiments in realistic scenarios. An initial back-to-back test has been performed to characterize the system. Then an experimental campaign was carried out in various environments at the School of Engineering and Computing Sciences, Durham University.

A. Proposed Radar System

Fig. 10 shows the block diagram of the proposed radar system. The system combines off-the-shelf RF components from Mini-Circuits with components which have been designed and manufactured ad hoc to meet the requirements. The arbitrary waveform generators (AWG) are the most important components as they generate the FMCW-FMICW signal at the transmitter and its replica to drive the mixer at the receiver. They are commercial modules Euvis AWG801, capable of generating waveforms with frequency up to 4 GHz. The AWG are programmed by a PC through an interface developed in MATLAB and C++ to select the waveform parameters. The FPGA board provides trigger signals to the AWG, ensuring the synchronization of the whole system by locking these signals to the common clock. The output of the AWG is fed into a low pass filter with pass-band up to 3.5 GHz (LPF1) in order to attenuate the residual clock of the AWG and the alias image at high frequency. These filters have been designed and manufactured using the facilities at the School of

Engineering and Computing Sciences, Durham University. They consist of a distributed design based on microstrip lines and printed on a substrate Rogers 4003. At the transmitter side the signal is fed into the amplifier ZHL-4240 (POW AMP), thus achieving about 28 dBm transmitted power. At the receiver the signal from the antenna is fed into the low noise amplifier ZX60-3011 (LNA) and the output multiplied by a replica of the transmitted signal. The multiplication is performed by the mixer ZEM-4300MH, and the amplifier ZKL-2R7 (AMP1) is used to drive the LO port of the mixer with the required power level, 13 dBm. The resulting beat-note signal is filtered to get the low frequency components carrying information on the distance of the targets. The filter has been manufactured with lumped components to get a cut-off frequency of 10 MHz. After filtering this signal is fed into the amplifier ZHL-6A (AMP2) and recorded by the 14 bit analogue-to-digital converter (ADC) Signatec PX14400A. The system operates in bistatic approach with one antenna at the transmitter and one at the receiver. Two different models of antennas have been designed and manufactured to work across the desired frequency bandwidth (0.7-2.2 GHz) and have a directional radiation pattern, so that the energy can be focused towards the wall and the targets to be detected, avoiding the reception of clutter and undesired signals from secondary lobes. These antennas are Antipodal Vivaldi and rectangular patch [32].

As mentioned, the frequency range of the waveforms used in the experimental campaign is 0.7-2.2 GHz, thus providing 10 cm range resolution and sufficient through-wall penetration for common construction material as bricks or concrete [1]. The duration of the FMCW-FMICW waveform is 400 μs. Higher values would give higher time-bandwidth product for the waveform, but they would increase the time to modify and load the waveform into the AWG; therefore this value is a good compromise to perform experiments. The minimum allowed sampling frequency of the ADC is 20 MHz, thus the maximum alias-free beat-note frequency is 10 MHz. The distance of the target corresponding to the maximum beat-note frequency would be 400 m with the aforementioned bandwidth and duration of the waveform. Therefore the beat-note components related to targets a few meters away from the radar system can be recorded with the parameters presented above.

Motion and breathing detection are performed through double FFT processing aimed at extracting the Doppler shifts caused by the movement [33]. Given the duration of the FMCW-FMICW waveforms, the maximum

Doppler shift without ambiguity is ±1250 Hz, which is far higher than the shift produced by movements or breathing of people. The Doppler resolution depends on the number of FMCW-FMICW waveforms which are processed to extract Doppler information, thus on the overall length of the data which are recorded in a measurement. For motion detection we recorded data for 10 s, corresponding to 0.1 Hz Doppler resolution, whereas for breathing detection we aimed at finer resolution to analyze the small movement of the chest, by recording 20 s of data, corresponding to 0.05 Hz resolution. With the aforementioned parameters and assuming maximum distance of the target 5 m, the anti-aliasing condition in (3) yields maximum bit duration 4μs/N for a N-bit gating sequence, more than enough for our experiments where relevant beat-note components are at tens of nanoseconds.

B. Comparison with other hardware approaches

As mentioned in section II, only hardware wall removal techniques like FMICW or band-pass filtering can solve the dynamic range issue.

The band-pass filtering approach employed in FMCW radar systems requires a filter centered at a suitable intermediate frequency and with high Q to have a steep transition between the stop and the pass bands [12]. An additional oscillator is then required to adapt the frequency of the beat-note signal to the fixed band of the band-pass filter, in case of changes due to different stand-off distances or different duration or bandwidth of the transmitted FMCW waveform.

In our system the AWG replaces the aforementioned components, as it can generate both FMCW and FMICW waveforms through a simple software interface. The great advantage of the AWG is its flexibility in changing the parameters of the waveforms, namely bandwidth and duration which impact on the beat-note frequency associated with a certain range of round-trip delay values. These parameters can take any value within the limit given by the particular model of AWG (in our case 4 GHz bandwidth and 1 ms duration), whereas the chirp duration provided by analogue methods of generation of FMCW signals such as Yttrium Garnet Iron (YIG) oscillators may be limited to a set of values depending on the controlling voltage ramp. The parameters of the gating sequence for FMICW waveforms, like type of sequence, bit duration, and additional delays τ_{RX1} and τ_{RX2}, can also be flexibly changed using the AWG. This provides gating sequences and MRS patterns

which can be adapted to different scenarios under test, for instance providing wider notches of the MRS to attenuate wall reflections from particularly challenging walls, or using a notch to attenuate a partition wall placed in the middle of the area under test, or enhancing the contributions from a far target or from a portion of the area under test by using a suitable square wave sequence (as shown in section III for the second simulated scenario). This flexibility provided by the AWG justifies its cost, although a comparison with other approaches in terms of cost strongly depends on the models of AWG and the oscillators, high linearity voltage ramp source, and band-pass filter chosen for the particular radar system.

Another possible approach is using gated SFCW signals, as shown in the system presented in [34] to remove the reflection from the air/ground interface for ground penetrating radar (GPR) applications. In this system, switches and delay circuits controlled by a digital synthesizer are used to gate the waveforms by using simple square waves as on-off patterns. Another synthesizer and phase-locked-loops are used to generate the SFCW waveform and convert it to the desired frequency range. In our system the AWG replaces the aforementioned components, allowing the flexible generation of FMCW and FMICW waveforms gated with different sequences. Furthermore, the required time for a complete trace in the SFCW system is around 75 ms because of the PLL setup and lock time. Although this is acceptable for GPR applications, it would result in poor Doppler resolution for movement detection, whereas our system provides suitable values and allows the exploitation of Doppler shifts recording for movement and breathing detection, as shown later in this section.

Even a time-gating device at the front-end of the receiver could tackle this issue, but, apart from its hardware complexity and related costs, it would be applicable only to pulse-based systems and not to systems based on frequency modulated waveforms. Our focus is on these systems as they generally require less expensive ADC at the receiver and lower transmitted peak power [12].

C. Back-to-back Test

In back-to-back tests the transmitter is directly connected to the receiver through cables giving different propagation delays and attenuation, without using antennas. The different propagation delays and attenuation simulate the presence of targets placed at different distances and with different RCS. We present one back-to-back test performed to characterize the system. We show the methodology used to design suitable FMICW

waveforms for wall removal during the experimental campaign. Compared with the diagram shown in Fig. 10, the antennas have been removed and the transmitted signal is split and fed into two propagation paths and then combined and fed into the receiver. The values of the attenuators for the two paths are 50 and 66 dB, plus additional attenuation caused by the cables.

Normal FMCW waveforms are initially used to identify the various frequency components in the beat-note spectrum, which is called range profile as the frequency is related to the delay and therefore to the range in FMCW based radar systems. In through-wall experiments the wall return is expected to be the strongest component and located at lower frequency, as the wall is closer to the radar system compared with the targets. In this back-to-back test two components are expected, one for each propagation path. Fig. 11 shows the range profile using FMCW and FMICW waveforms, with the former presenting two components at values of delay 21.17 ns and 33.78 ns. These delays include the internal delay inside the hardware components of the radar system.

Assuming that the first component would be the undesired return from the wall in a realistic experiment, a suitable gating sequence can be designed to remove it through FMICW waveforms. The gating sequence is the 3 bit M-sequence with bit duration 30 ns, delay τ_{RX1} equal to 0 ns, and delay τ_{RX2} equal to 21.125 ns. The MRS of this sequence is shown in Fig. 3. The first blind range mitigates the first component in the range profile, whereas the second component is located in the flat area of the MRS where no additional attenuation is provided. As a result, in the FMICW range profile shown in Fig. 11 the second component is the strongest. When using normal FMCW waveforms the first component is about 12 dB higher than the second one, whereas when using the proposed FMICW waveforms the second component is about 20 dB higher than the residual of the first one.

D. Detection of Stationary Targets

The effectiveness of the proposed FMICW waveforms for the through-wall detection of stationary targets has been tested with several objects. In this paper a fire extinguisher is used as target. Fig. 12 shows the fire extinguisher placed inside a meeting room containing also office-like pieces of furniture such as chairs and tables. The radar system is placed outside the room, behind the wall shown on the right-hand side of Fig. 12.

The wall is made of plastered plywood panels with an internal honeycomb structure made of cardboard. The wall is 8 cm thick and its permittivity is assumed to be 1.6, a sort of average between the value of the plywood and the value of air.

Fig. 13 presents two radar profiles for this experimental scenario, using FMCW and FMICW waveforms respectively. In both cases the signals have been recorded at a position in line with the target and are normalized to the maximum of the FMCW profile, which is the reflection from the wall located at round-trip delay 20.8 ns. The gating sequence used for the FMICW waveforms is the 3 bit M-sequence with bit duration 7 ns and delays τ_{RX1} and τ_{RX2} equal to 0.75 ns. These values produce the MRS pattern shown in Fig. 3, with the second blind range which is centered at 21 ns and 1.5 ns long, thus suitable to attenuate the unwanted component at 20.8 ns so that the reflection from the target is the strongest component in the FMICW profile. Unlike the simulated profiles in Fig. 6, in the experiments the FMICW profile has been properly amplified with the full dynamic range of the digitizer applied to the area under test behind the wall. This allows compensating for the additional attenuation due to the off-time at the receiver.

Fig. 14 shows radar images created for this scenario using FMCW and FMICW waveforms and different imaging algorithms. The data have been collected in synthetic aperture radar (SAR) approach while moving the antennas along an array of 7 positions located 10 cm apart. For each position the distance between the two antennas is 20 cm and the stand-off distance from the wall about 1 cm. In the FMCW case (Fig. 14a) wall reflections are the strongest return in the image and the target contribution appears not easily distinguishable from the clutter, as it could be expected looking also at the FMCW profile in Fig. 13. In the FMICW case the reflection from the fire extinguisher is the strongest and brightest contribution in the image, with the wall residual at least 25 dB below it. Comparing Fig. 14b with 14c and 14d we can see how DSI and even more DMSI algorithms help to focus the coloured spots on the actual positions of the target. In this case they also strongly attenuate (in case of DSI) or remove (in case of DMSI) the artefact at roughly 50 cm down-range, which is present in Fig. 14b when using BP algorithm.

E. Detection of Movement: Walking and Breathing

FMICW waveforms have been validated in experiments to detect the presence of people behind walls through their movements or breathing. The experiments have been performed in two environments at the School of Engineering and Computing Science, Durham University. One environment is an open landing separated by a 16 cm brick wall from a corridor, the other is a teaching room with 25 cm concrete walls. The presence of movement is detected through Doppler shifts, which are extracted from the data through double FFT processing and shown in Delay-Doppler patterns.

Fig. 15 shows Delay-Doppler patterns for a person walking with fast pace behind the brick wall on a radial trajectory when FMCW (sub-figure 15a) and FMICW (sub-figure 15b) waveforms are used. Fig. 16 presents the same comparison for the case when the person is standing and swinging arms. The color scales are the same in every sub-figure in Fig. 15 and 16, with maximum magnitude value assigned to the wall reflections in the FMCW case. The gating sequence used for FMICW waveforms is a 3 bit M-sequence with bit duration 26 ns and delay τ_{RX2} equal to 21.5ns, which is the round-trip delay related to the undesired reflection from the wall. This reflection appears in both figures 15a and 16a as an orange bright spot at 21.5 ns and 0 Hz Doppler when FMCW waveforms are used. Compared with FMCW, the effectiveness of the FMICW waveforms can be seen as they improve the detection of the Doppler shifts produced by both types of movement. Walking produces Doppler shifts up to roughly ±15 Hz at values of delay in the interval 25-35 ns. This corresponds to a walking speed of about 3 m/s and at distances in the interval 70-220 cm from the radar system, which is compatible with the performed experiment. The movement of arms produces a Doppler shift more localized in terms of delay, as the person is standing, and the entity of the shift is smaller compared with walking as the movement of arms is a bit slower.

Fig. 17 and 18 show Delay-Doppler patterns from the experiments performed in the scenario with concrete walls. In this case only FMICW waveforms have been used, as the aim is presenting the Doppler patterns of different kinds of movements in the same scenario rather than comparing FMCW-FMICW waveforms. These sub-figures in Fig. 17 and 18 are plotted using the same color scale with normalization to the wall reflection in

case of FMCW signal, so that the residual wall return and static clutter appear at around -20 dB, and the Doppler shifts at about –40 dB.

The gating sequence is the 3 bit M-sequence with bit duration 34 ns and delay τ_{RX2} equal to 28 ns. In comparison with the brick wall scenario it is necessary to increase the delay τ_{RX2}, thus extending the blind range of the MRS for more effective wall removal, since the reflection from the concrete wall is spread across a longer interval, as the concrete wall is thicker and with higher permittivity. Fig. 17a shows the Delay-Doppler pattern for an empty scenario and as expected only stationary components at 0 Hz are present. Fig. 17b refers to the scenario where a person is standing and moving hands, as if during an animate conversation. As expected the Doppler shift is localized in terms of round-trip delay (at roughly 32 ns) as the person is standing at a fixed distance from the radar, and the entity of the Doppler is small (roughly ±3 Hz) as the movement speed is small. In Fig. 18 the patterns for a person walking on two different trajectories is shown. In Fig. 18a the trajectory is radial, thus generating the highest Doppler shift, whereas in Fig. 18b the trajectory is diagonal and as expected the value of the Doppler is smaller (around ±10 Hz against ±20 Hz in the previous case).

FMICW waveforms have been also used for experiments aiming at detecting the presence of people behind walls through the Doppler shift caused by the chest movement while breathing. This shift is far smaller than those seen for walking or for limbs movements, around 0.2-0.33 Hz for normal respiration rates in adults and depending on the physical condition of the person [35]. Fig. 19 shows Delay-Doppler patterns referring to tests where the person is standing behind the brick wall and breathing at fast (figures 19a and 19b) and normal pace (figures 19c and 19d). For both situations the patterns using normal FMCW and proposed FMICW waveforms are shown. Only the contribution from the stationary background can be seen in the former case, including wall reflections which appear as a yellow bright spot at delay 21.5 ns. FMICW waveforms are effective in mitigating the stationary contribution, thus allowing the detection of the Doppler shift caused by breathing. As expected this shift is higher (roughly up to ±1 Hz) for faster breathing rate in figure 19b and lower for normal rate (around ±0.5 Hz) as in figure 19d. In both cases the shift is located at roughly 28 ns delay, as the person is standing at a fixed distance from the radar while breathing.

Fig. 20 presents Delay-Doppler patterns with reference to the scenario with concrete walls and normal and slow breathing rate. Fig. 20a and 20b compares the pattern for the normal rate when using FMCW and FMICW waveforms, respectively. The breathing Doppler shift can be detected only when using FMICW waveforms, otherwise only the contribution of the stationary background and wall is detected. Fig. 20c and 20d shows the same comparison referring to the case of slow breathing rate; the Doppler shift can be seen only when FMICW waveforms are used. As expected the Doppler shift for the slow rate is smaller than the case of fast rate, roughly ±0.2 Hz against ±0.5 Hz.

V- CONCLUSIONS

In this paper we have presented FMICW waveforms as a novel wall removal technique for through-wall detection. Wall reflections can be mitigated and the detection of targets improved by choosing suitable gating sequences to generate the proposed FMICW waveforms. Validation has been provided through numerical simulations and experimental results obtained using a radar system built for the purpose and capable of flexibly generating FMICW waveforms through AWGs. Results for through-wall detection of stationary targets and of people through their movement and breathing have been presented.

Further work could be carried out to upgrade the current bistatic system with an array of antennas and related switching and control units which would provide faster creation of images in comparison with the SAR approach, and also the possibility to locate and track moving targets. The possibility of combining FMICW waveforms with other wall removal techniques, such as subspace projection, spatial filtering, and change detection, could be also investigated.

ACKNOWLEDGMENT

The authors would like to thank Her Majesty's Government Communications Centre (HMGCC) for the sponsorship of this project.

REFERENCES

[1] M. Farwell, *et al.*, "Sense through the wall system development and design considerations," *Journal of the Franklin Institute*, vol. 345, pp. 570-591, 2008.

[2] Y. Wang, *et al.*, "Simultaneous localization and respiration detection of multiple people using low cost UWB biometric pulse Doppler radar sensor," in *Microwave Symposium Digest (MTT), 2012 IEEE MTT-S International*, 2012, pp. 1-3.

[3] W. Shiyou, *et al.*, "A simple strategy for moving target imaging via an experimental UWB through-wall radar," in *Ground Penetrating Radar (GPR), 2012 14th International Conference on*, 2012, pp. 961-965.

[4] K. Ranney, *et al.*, "Recent MTI experiments using ARL's synchronous impulse reconstruction (SIRE) radar," 2008, p. 694708.

[5] C. Pin-Heng, *et al.*, "A portable real-time digital noise radar system for through-the-wall imaging," *Geoscience and Remote Sensing, IEEE Transactions on*, vol. 50, pp. 4123-4134, 2012.

[6] J. Sachs, *et al.*, "Detection and tracking of moving or trapped people hidden by obstacles using ultra-wideband pseudo-noise radar," in *Radar Conference, 2008. EuRAD 2008. European*, 2008, pp. 408-411.

[7] K. E. Browne, *et al.*, "Through-wall opportunistic sensing system utilizing a low-cost flat-panel array," *Antennas and Propagation, IEEE Transactions on*, vol. 59, pp. 859-868, 2011.

[8] L. Biying, *et al.*, "A SFCW radar for through wall imaging and motion detection," in *Radar Conference (EuRAD), 2011 European*, 2011, pp. 325-328.

[9] L. Biying, *et al.*, "Detection of human beings in motion behind the wall using SAR interferogram," *Geoscience and Remote Sensing Letters, IEEE*, vol. 9, pp. 968-971, 2012.

[10] N. Maaref and P. Millot, "Array-based UWB FMCW through-the-wall radar," in *Antennas and Propagation Society International Symposium (APSURSI), 2012 IEEE*, 2012, pp. 1-2.

[11] N. Maaref and P. Millot, "Array-based ultrawideband through-wall radar: prediction and assessment of real radar abilities," *International Journal of Antennas and Propagation*, vol. 2013, p. 9, 2013.

[12] G. L. Charvat, *et al.*, "A through-dielectric radar imaging system," *Antennas and Propagation, IEEE Transactions on*, vol. 58, pp. 2594-2603, 2010.

[13] G. L. Charvat, *et al.*, "A through-dielectric ultrawideband (UWB) switched-antenna-array radar imaging system," *Antennas and Propagation, IEEE Transactions on*, vol. 60, pp. 5495-5500, 2012.

[14] T. S. Ralston, *et al.*, "Real-time through-wall imaging using an ultrawideband multiple-input multiple-output (MIMO) phased array radar system," in *Phased Array Systems and Technology (ARRAY), 2010 IEEE International Symposium on*, 2010, pp. 551-558.

[15] J. Peabody, *et al.*, "Through-Wall Imaging Radar," *Lincoln Laboratory Journal*, vol. 19, pp. 62-72, 2012.

[16] Y. Yeo-Sun and M. G. Amin, "Spatial filtering for wall-clutter mitigation in through-the-wall radar imaging," *Geoscience and Remote Sensing, IEEE Transactions on*, vol. 47, pp. 3192-3208, 2009.

[17] J. Qian, *et al.*, "Joint localization of stationary and moving targets behind walls using sparse scene recovery," *Journal of Electronic Imaging*, vol. 22, pp. 021002-021002, 2013.

[18] A. N. Gaikwad, *et al.*, "Application of clutter reduction techniques for detection of metallic and low dielectric target behind the brick wall by stepped frequency continuous wave radar in ultra-wideband range," *Radar, Sonar & Navigation, IET*, vol. 5, pp. 416-425, 2011.

[19] F. H. C. Tivive, *et al.*, "An SVD-based approach for mitigating wall reflections in through-the-wall radar imaging," in *Radar Conference (RADAR), 2011 IEEE*, 2011, pp. 519-524.

[20] M. Dehmollaian and K. Sarabandi, "Refocusing through building walls using synthetic aperture radar," *Geoscience and Remote Sensing, IEEE Transactions on*, vol. 46, pp. 1589-1599, 2008.

[21] T. Dogaru and C. Le, "SAR images of rooms and buildings based on FDTD computer models," *Geoscience and Remote Sensing, IEEE Transactions on*, vol. 47, pp. 1388-1401, 2009.

[22] M. G. Amin, *Through-the-Wall Radar Imaging*: CRC Press, 2010.

[23] S. Salous, *Radio Propagation Measurement and Channel Modelling*: Wiley, 2013.

[24] S. Fujii, *et al.*, "An overview of developments and applications of oceanographic radar networks in Asia and Oceania countries," *Ocean Science Journal*, vol. 48, pp. 69-97, 2013/03/01 2013.

[25] A. Poole, "On the use of pseudorandom codes for "Chirp" radar," *Antennas and Propagation, IEEE Transactions on*, vol. 27, pp. 480-485, 1979.

[26] T. Dogaru and C. Le, "Simulated radar range profiles of a simple room as computed by FDTD and Xpatch," Army Research Laboratory, Adelphi, MD Tech. Rep. ARL-TR-4420, 2008.

[27] T. Dogaru, *et al.*, "Computer Models of the Human Body Signature for Sensing Through the Wall Radar Applications," Army Research Laboratory, Adelphi, MD, Tech. Rep. ARL-TR-4290, 2007.

[28] L. Chen and O. Shan, "Through-wall surveillance using ultra-wideband short pulse radar: numerical simulation," in *Industrial Electronics and Applications, 2007. ICIEA 2007. 2nd IEEE Conference on*, 2007, pp. 1551-1554.

[29] L. Hooi Been, *et al.*, "Confocal microwave imaging for breast cancer detection: delay-multiply-and-sum image reconstruction algorithm," *Biomedical Engineering, IEEE Transactions on*, vol. 55, pp. 1697-1704, 2008.

[30] D. Byrne, *et al.*, "Data independent radar beamforming algorithms for breast cancer detection," *Progress in Electromagnetic Research*, vol. 107, pp. 331-348, 2010.

[31] F. Ahmad, *et al.*, "Synthetic aperture beamformer for imaging through a dielectric wall," *Aerospace and Electronic Systems, IEEE Transactions on*, vol. 41, pp. 271-283, 2005.

[32] F. Fioranelli, *et al.*, "Optmized patch-like antennas for through the wall radar imaging and preliminary results with frequency modulated interrupted continuous wave," in *Signals, Systems, and Electronics (ISSSE), 2012 International Symposium on*, 2012, pp. 1-5.

[33] D. E. Barrick, *FM/CW radar signals and digital processing*: Environmental Research Laboratories, 1973.

[34] M. J. Oyan, *et al.*, "Ultrawideband gated step frequency ground-penetrating radar," *Geoscience and Remote Sensing, IEEE Transactions on*, vol. 50, pp. 212-220, 2012.

[35] J. Sachs, *et al.*, "Remote vital sign detection for rescue, security, and medical care by ultra-wideband pseudo-noise radar," *Ad Hoc Networks*, 2012.

FIGURES

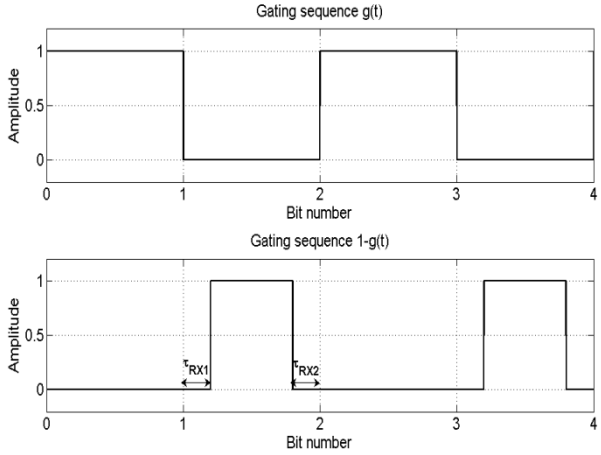

Fig. 1 Bit pattern of the square wave

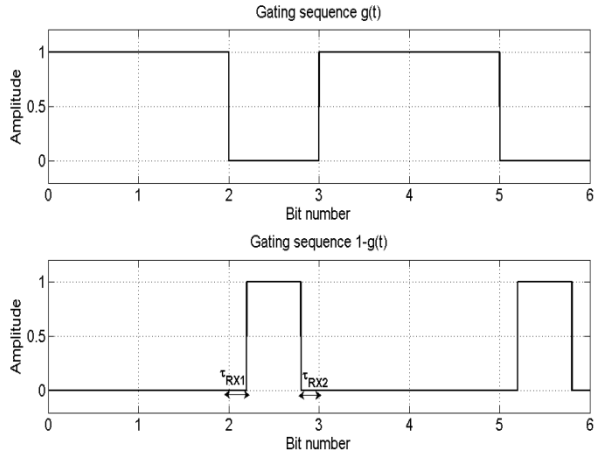

Fig. 2 Bit pattern of the 3 bit M-sequence

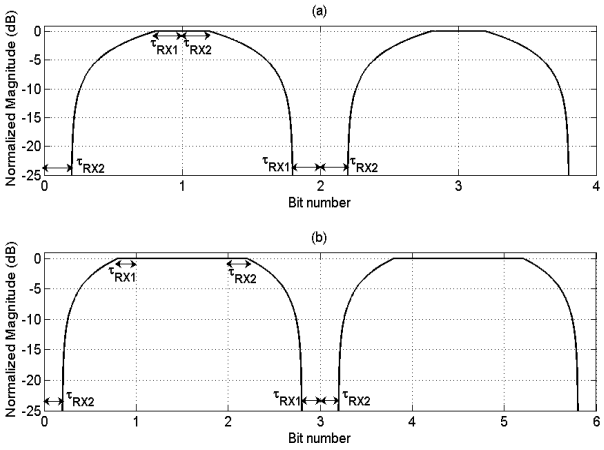

Fig. 3 MRS of the square wave (a) and of the 3 bit M-sequence (b)

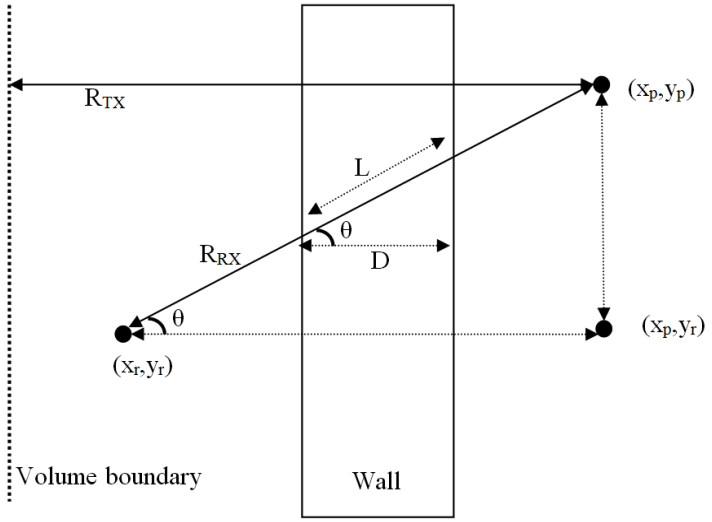

Fig. 4 Simplified geometry of the through-wall scenario for θ estimation

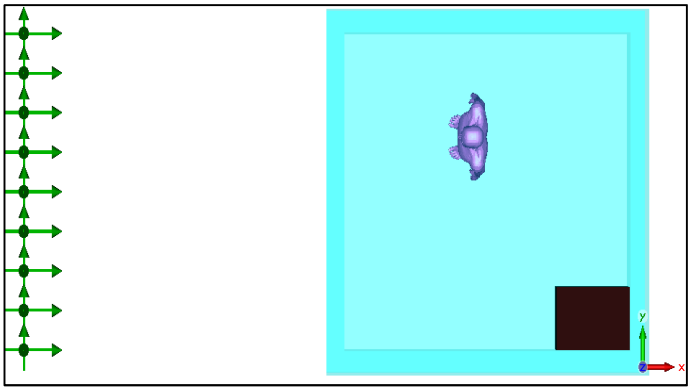

Fig. 5 First simulated scenario with probes and targets inside the room

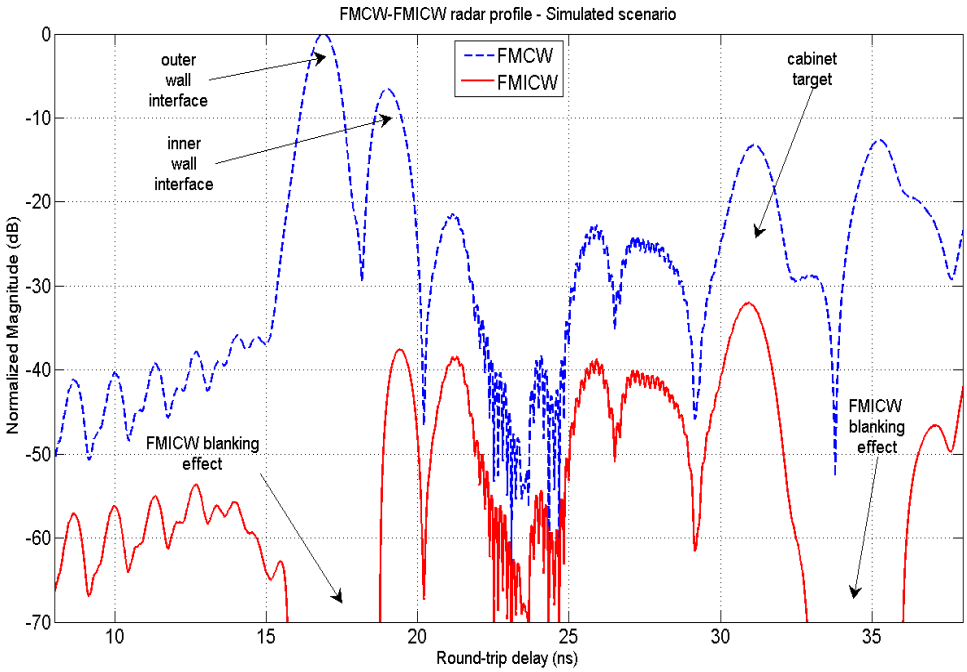

Fig. 6 FMCW and FMICW range profiles for the first simulated scenario

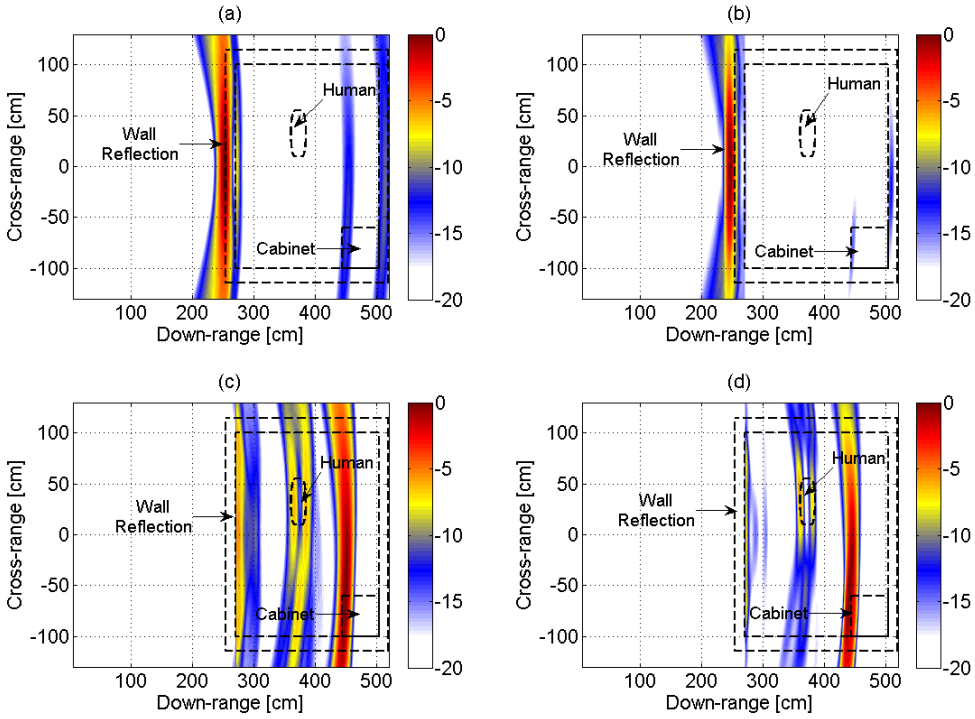

Fig. 7 Radar images for the first simulated scenario: (a) using FMCW and BP algorithm, (b) using FMCW and DMSI algorithm, (c) using FMICW and BP algorithm, and (d) using FMICW and DMSI algorithm.

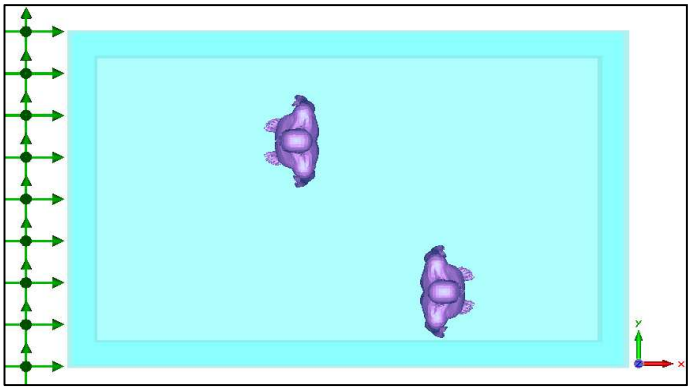

Fig. 8 Second simulated scenario with probes and targets inside the room

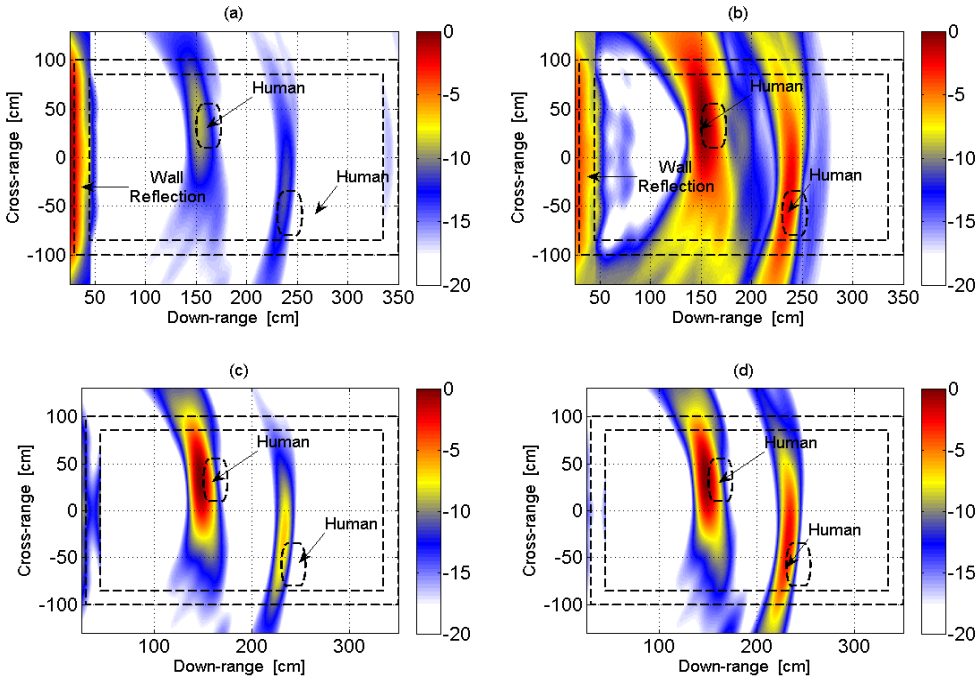

Fig. 9 Radar images for the second simulated scenario: (a) using FMCW and BP algorithm, (b) using FMICW with M-sequence and BP algorithm, (c) using FMICW with M-sequence and DMSI algorithm, and (d) using FMICW with square wave and DMSI algorithm

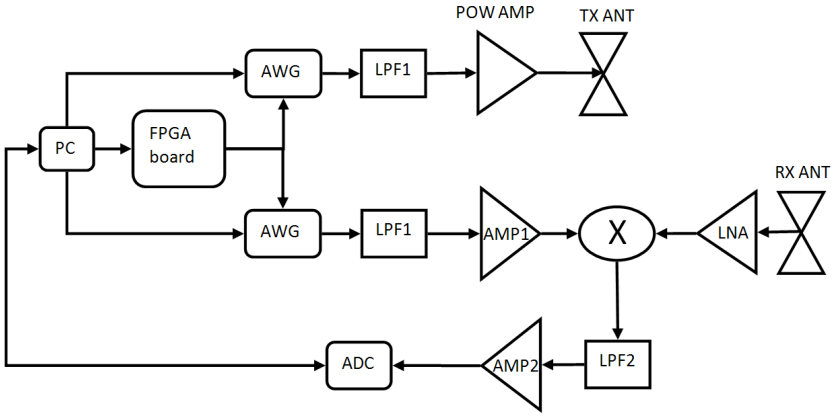

Fig. 10 Block diagram of the proposed radar system

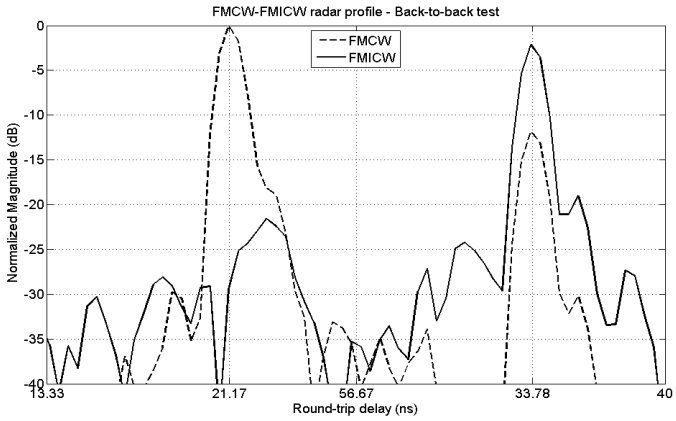

Fig. 11 FMCW and FMICW range profiles for the back-to-back test

Fig. 12 View of the experimental setup with stationary target inside the room behind plastered plywood wall

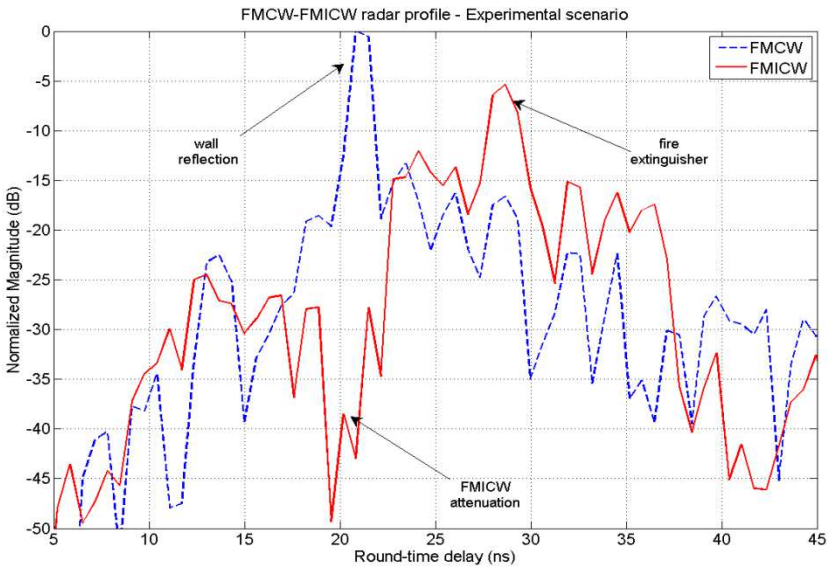

Fig. 13 FMCW and FMICW range profiles for the experimental scenario

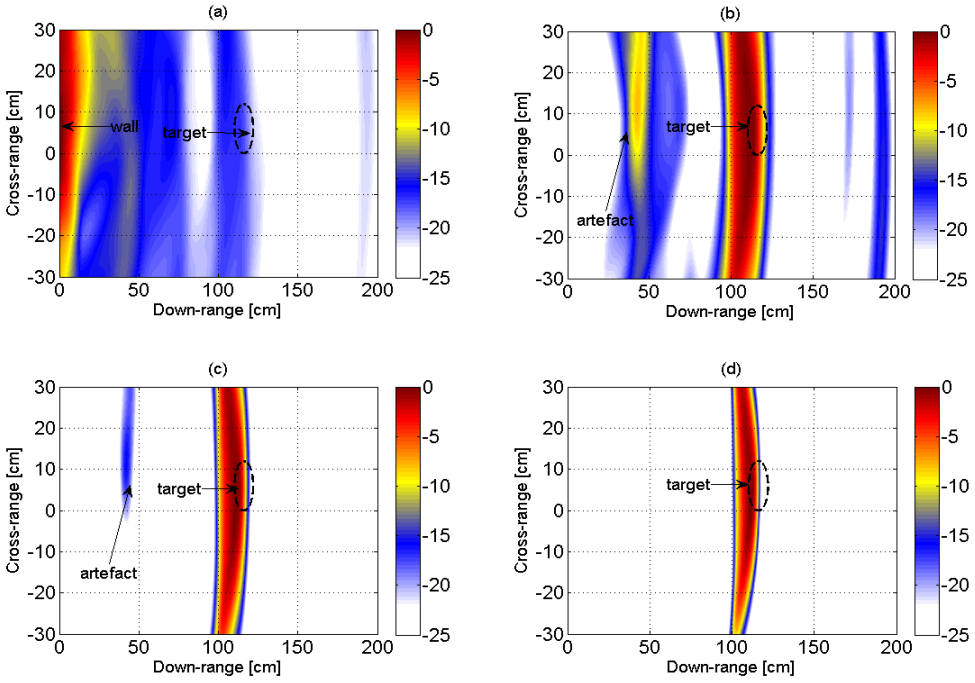

Fig. 14 Radar images for detection of the stationary target: (a) using FMCW and BP algorithm, (b) using FMICW and BP algorithm, (c) using FMICW and DSI algorithm, and (d) using FMICW and DMSI algorithm

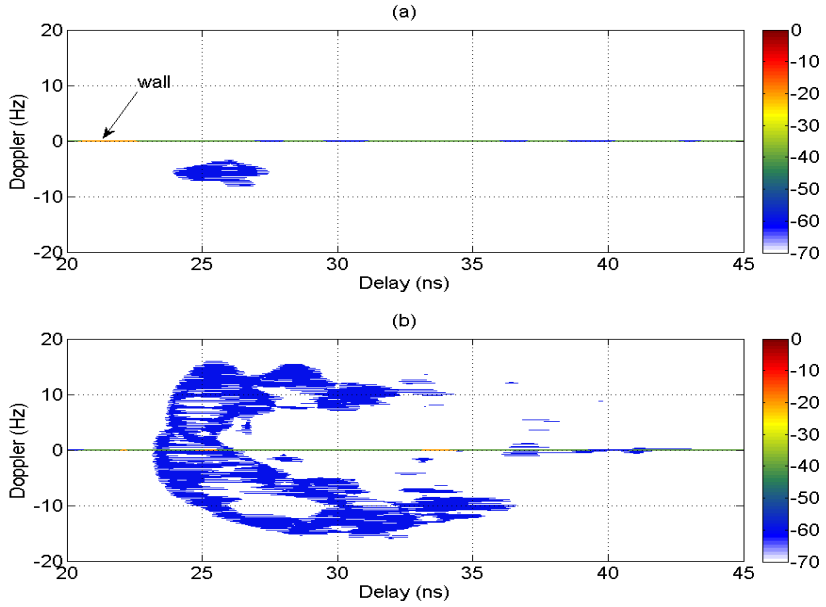

Fig. 15 Delay-Doppler for detection of a person walking behind brick wall: (a) using FMCW, and (b) using FMICW waveforms

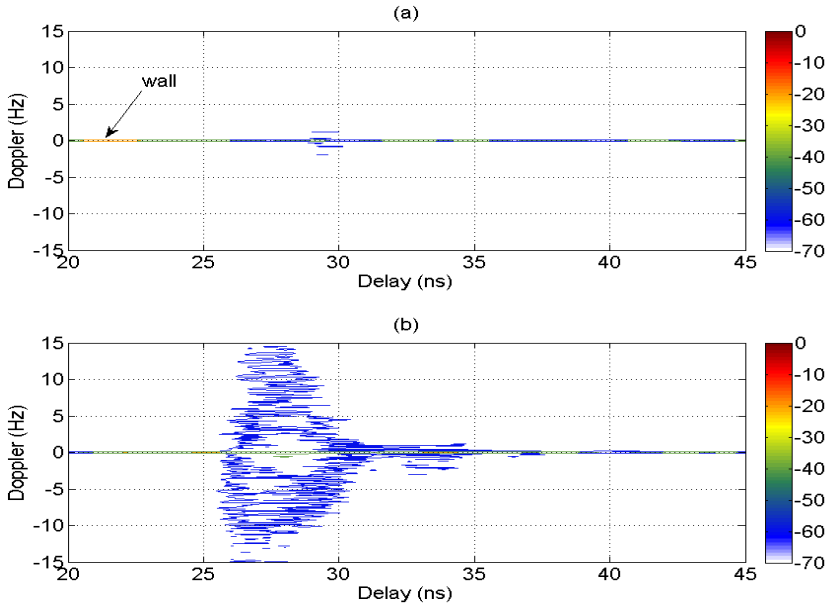

Fig. 16 Delay-Doppler for detection of a person standing and swinging arms behind brick wall: (a) using FMCW, and (b) using FMICW waveforms

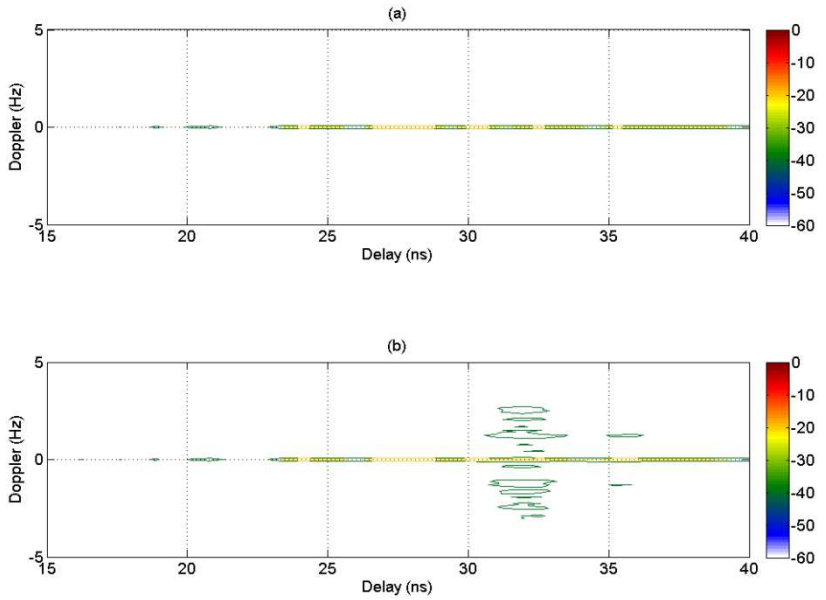

Fig. 17 Delay-Doppler for movement detection behind concrete wall using FMICW waveforms: (a) empty scenario, and (b) person standing and moving hands

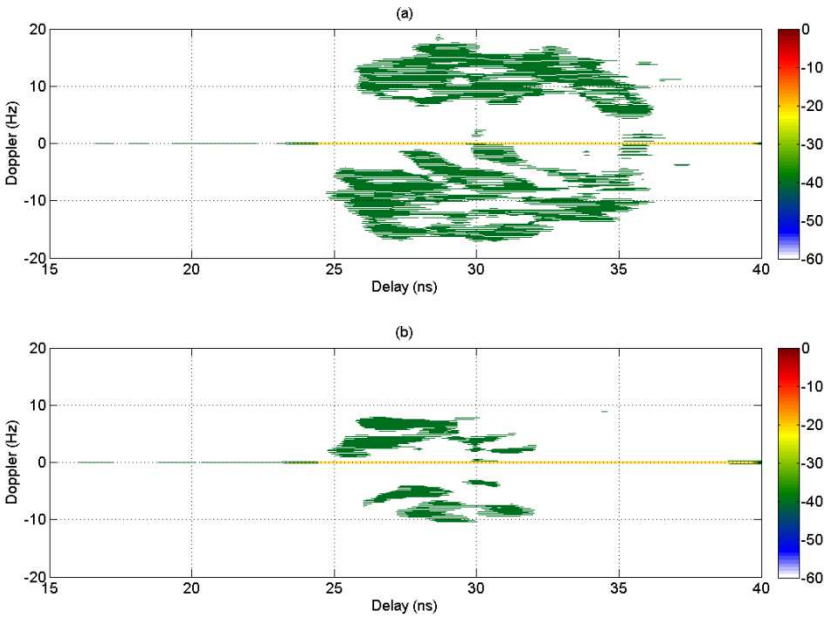

Fig. 18 Delay-Doppler for movement detection behind concrete wall using FMICW waveforms: (a) person walking on radial trajectory, and (b) person walking on diagonal trajectory

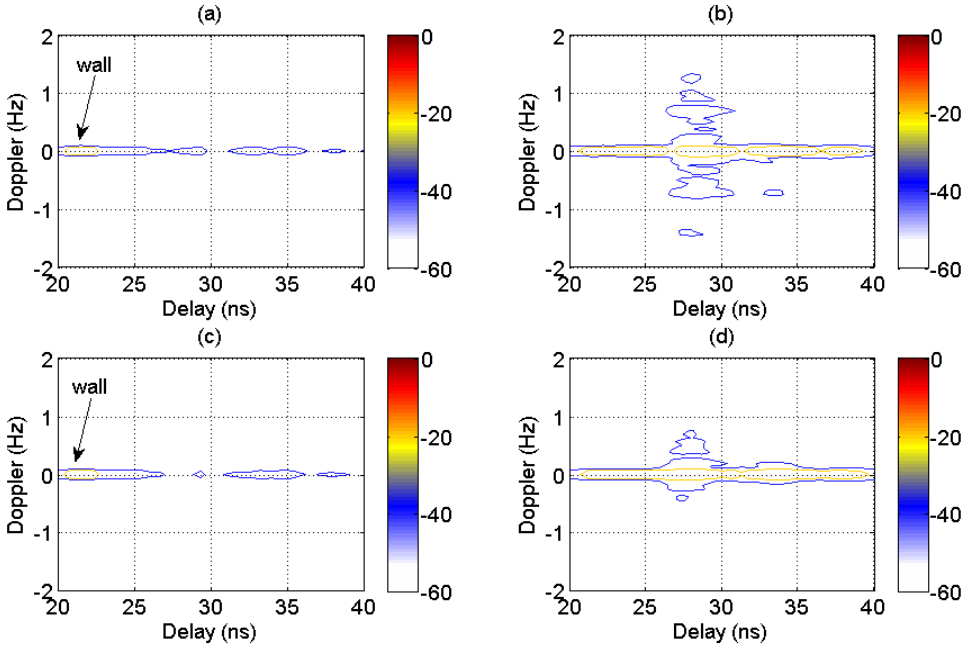

Fig. 19 Delay-Doppler for breathing detection behind brick wall: (a) fast breathing rate using FMCW, (b) fast breathing rate using FMICW, (c) normal breathing rate using FMCW, and (d) normal breathing rate using FMICW

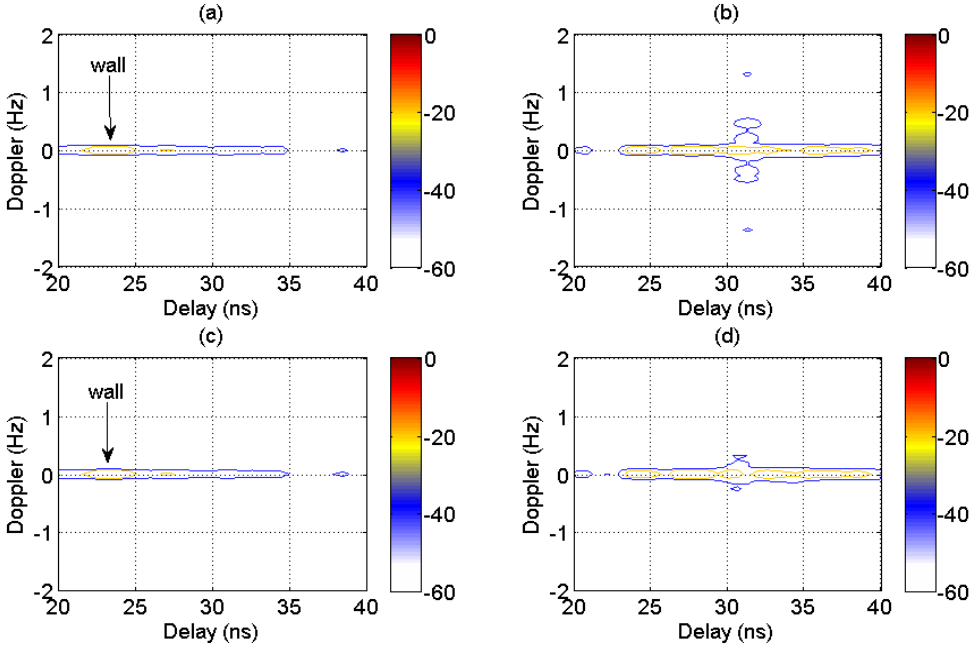

Fig. 20 Delay-Doppler for breathing detection behind concrete wall: (a) normal breathing rate using FMCW, (b) normal breathing rate using FMICW, (c) slow breathing rate using FMCW, and (d) slow breathing rate using FMICW

FIGURE CAPTIONS

Fig. 12 Bit pattern of the square wave

Fig. 13 Bit pattern of the 3 bit M-sequence

Fig. 14 MRS of the square wave (a) and of the 3 bit M-sequence (b)

Fig. 15 Simplified geometry of the through-wall scenario for θ estimation

Fig. 16 First simulated scenario with probes and targets inside the room

Fig. 17 FMCW and FMICW range profiles for the first simulated scenario

Fig. 18 Radar images for the first simulated scenario: (a) using FMCW and BP algorithm, (b) using FMCW and DMSI algorithm, (c) using FMICW and BP algorithm, and (d) using FMICW and DMSI algorithm.

Fig. 19 Second simulated scenario with probes and targets inside the room

Fig. 20 Radar images for the second simulated scenario: (a) using FMCW and BP algorithm, (b) using FMICW with M-sequence and BP algorithm, (c) using FMICW with M-sequence and DMSI algorithm, and (d) using FMICW with square wave and DMSI algorithm

Fig. 21 Block diagram of the proposed radar system

Fig. 22 FMCW and FMICW range profiles for the back-to-back test

Fig. 12 View of the experimental setup with stationary target inside the room behind plastered plywood wall

Fig. 13 FMCW and FMICW range profiles for the experimental scenario

Fig. 14 Radar images for detection of the stationary target: (a) using FMCW and BP algorithm, (b) using FMICW and BP algorithm, (c) using FMICW and DSI algorithm, and (d) using FMICW and DMSI algorithm

Fig. 15 Delay-Doppler for detection of a person walking behind brick wall: (a) using FMCW, and (b) using FMICW waveforms

Fig. 16 Delay-Doppler for detection of a person standing and swinging arms behind brick wall: (a) using FMCW, and (b) using FMICW waveforms

Fig. 17 Delay-Doppler for movement detection behind concrete wall using FMICW waveforms: (a) empty scenario, and (b) person standing and moving hands

Fig. 18 Delay-Doppler for movement detection behind concrete wall using FMICW waveforms: (a) person walking on radial trajectory, and (b) person walking on diagonal trajectory

Fig. 19 Delay-Doppler for breathing detection behind brick wall: (a) fast breathing rate using FMCW, (b) fast breathing rate using FMICW, (c) normal breathing rate using FMCW, and (d) normal breathing rate using FMICW

Fig. 20 Delay-Doppler for breathing detection behind concrete wall: (a) normal breathing rate using FMCW, (b) normal breathing rate using FMICW, (c) slow breathing rate using FMCW, and (d) slow breathing rate using FMICW